Vol. 41 — N° 4 12 17 p. 633 – 647

GEOSTANDARDS and GEOANALYTICAL RESEARCH

Separation of Platinum from Palladium and Iridium in Iron Meteorites and Accurate High-Precision Determination of Platinum Isotopes by Multi-Collector ICP-MS

Alison C. **Hunt*** , Mattias **Ek** and Maria **Schönbächler**

Institute of Geochemistry and Petrology, ETH Zürich, Clausiusstrasse 25, Zürich 8092, Switzerland
* Corresponding author. e-mail: alison.hunt@erdw.ethz.ch

This study presents a new measurement procedure for the isolation of Pt from iron meteorite samples. The method also allows for the separation of Pd from the same sample aliquot. The separation entails a two-stage anion-exchange procedure. In the first stage, Pt and Pd are separated from each other and from major matrix constituents including Fe and Ni. In the second stage, Ir is reduced with ascorbic acid and eluted from the column before Pt collection. Platinum yields for the total procedure were typically 50–70%. After purification, high-precision Pt isotope determinations were performed by multi-collector ICP-MS. The precision of the new method was assessed using the IIAB iron meteorite North Chile. Replicate analyses of multiple digestions of this material yielded an intermediate precision for the measurement results of 0.73 for ε^{192}Pt, 0.15 for ε^{194}Pt and 0.09 for ε^{196}Pt (2 standard deviations). The NIST SRM 3140 Pt solution reference material was passed through the measurement procedure and yielded an isotopic composition that is identical to the unprocessed Pt reference material. This indicates that the new technique is unbiased within the limit of the estimated uncertainties. Data for three iron meteorites support that Pt isotope variations in these samples are due to exposure to galactic cosmic rays in space.

Keywords: Pt isotopes, Pd isotopes, multi-collector ICP-MS, ion-exchange chemistry, iron meteorites.

Received 13 Jan 17 – Accepted 09 May 17

Platinum is a platinum-group element (PGE; also Ru, Rh, Pd, Os and Ir) with six isotopes (^{190}Pt, ^{192}Pt, ^{194}Pt, ^{195}Pt, ^{196}Pt and ^{198}Pt; Table 1). It principally occurs as Pt^0, Pt^{2+} and Pt^{4+} in the Earth, but can also exist in a range of other oxidation states (Cotton *et al.* 1999). It is refractory, with a 50% condensation temperature of 1408 K (Lodders 2003). In common with all PGEs, Pt is highly siderophile and therefore strongly partitioned into the metal phase during core formation.

The applications of Pt isotopes are potentially very diverse. Mass-dependent isotope analyses may help to constrain terrestrial core formation and the late addition of extra-terrestrial materials to the Earth's mantle (Creech *et al.* 2017). Moreover, stable Pt isotope techniques may also be applied as a redox tracer in marine environments, as environmental monitors of vehicle emissions (Creech *et al.* 2013), and also to medical applications, where Pt-based compounds with various oxidation states are used as chemotherapy drugs (Cotton *et al.* 1999).

In this study, however, we focus on the improvement of analytical techniques for mass-independent Pt isotope amount ratio determinations, although our new separation technique may also be relevant for mass-dependent isotope determinations. Mass-independent Pt isotope determinations are a novel tool of increasing importance in cosmochemistry. This is because recently, Pt isotopes were established as a powerful neutron capture dosimeter (Leya and Masarik 2013). Neutron capture reactions in meteorites are a result of exposure to galactic cosmic rays (GCR) in space and can modify isotope ratios. Cosmogenic noble gases have traditionally been used to correct for GCR effects (e.g., Markowski *et al.* 2006), but their production occurs mainly at energies > 1 Me (Leya *et al.* 2000) and near the surface of meteoroids. Neutron capture occurs in the epithermal to thermal energy ranges (0.025 eV–10 keV), and its effects are greater deeper in the meteoroid. Neutron capture affects Pt and isotopes important for short-lived dating systems (i.e., ^{182}Hf-^{182}W

doi: 10.1111/ggr.12176

Table 1.
Relative abundance, nucleosynthetic production sites and major interferences for Pt isotopes

Isotopes	^{190}Pt	^{192}Pt	^{194}Pt	^{195}Pt	^{196}Pt	^{198}Pt
Relative abundance (%) [a]	0. 012	0.782	32.86	33.78	25.21	7.356
Nucleosynthetic production sites and % of contribution [b]	*p- (100.0)*	*s- (87.1)* *r- (12.9)*	*r- (93.4)* *s- (6.6)*	*r- (97.4)* *s- (2.6)*	*r- (86.8)* *s- (13.2)*	*r- (100.0)*
Major isobaric interferences and relative abundance (%) [c]	^{190}Os (26.26)	^{192}Os (40.78) ^{191}Ir (37.3)	^{193}Ir (62.7)		^{196}Hg (0.15)	^{198}Hg (9.97)

[a] Platinum abundance is taken from Wolff Briche *et al.* (2002); [b] *s*- and *r*-process contributions to Pt isotopes are taken from Bisterzo *et al.* (2011). [c] Ir, Os and Hg abundances from Berglund and Wieser (2011).

and ^{107}Pd-^{107}Ag; Masarik 1997, Leya and Masarik 2013). This indicates that Pt isotopes are important dosimeters for quantifying neutron capture effects on other isotopes (Kruijer *et al.* 2013, 2014, Wittig *et al.* 2013, Matthes *et al.* 2015). For example, the short-lived ^{182}Hf-^{182}W decay system is an important chronometer to constrain the timing of metal silicate separation in the early solar system. However, the W isotope data are affected by both the ingrowth of radiogenic ^{182}W and exposure to GCR (e.g., Kleine *et al.* 2005, Markowski *et al.* 2006). Platinum isotopes can be applied to monitor and correct for GCR-induced W isotope shifts, such that reliable ^{182}Hf-^{182}W ages are obtained (Kruijer *et al.* 2013, 2014, Wittig *et al.* 2013). In this approach, 'pre-GCR exposure' W isotope ratios are determined by empirical correlation of GCR-induced offsets in W and Pt isotopes, thereby allowing the determination of metal-silicate separation ages with small uncertainties. Additionally, Pt isotopes can be used for the correction of neutron capture-induced effects to various elements (e.g., Ru and Pd) to allow for the accurate assessment of nucleosynthetic isotope variations (Fischer-Gödde *et al.* 2015, Mayer *et al.* 2015, Ek *et al.* 2017, Fischer-Gödde and Kleine 2017).

Additionally, Pt isotopes can help to determine the nucleosynthetic sources of solar system materials and the potential heterogeneous distribution of material from these sources in our solar system. Elements heavier than Fe, including Pt, are mainly produced by neutron capture reactions (*s*- and *r*-processes; Table 1) that take place during the final stages of a stars' lifetime. Since Pt isotopes are produced by different nucleosynthetic processes (Table 1), they are useful for assessing the mechanisms that affected the delivery and distribution of these nuclides in our solar system. This includes (i) the heterogeneous injection of new material and inefficient mixing during the early evolution of our solar system (Vanhala and Boss 2002, Dauphas *et al.* 2004) and (ii) processing of presolar dust carrying unique nucleosynthetic signatures in the protoplanetary disc (Trinquier *et al.* 2009, Burkhardt *et al.* 2012, Akram *et al.* 2015, Mayer *et al.* 2015). Previous Pt isotope studies indicate *s*- and *r*-process homogeneity between different iron meteorite groups, within measurement uncertainty (Kruijer *et al.* 2013, 2014, Wittig *et al.* 2013, Peters *et al.* 2015). This corresponds well to studies of other heavy nuclides such as Hf and Os (Sprung *et al.* 2010, Walker 2012). However, lighter nuclides such as Pd, Ru and Zr show nucleosynthetic isotope variations (Akram *et al.* 2013, 2015, Fischer-Gödde *et al.* 2015, Mayer *et al.* 2015, Fischer-Gödde and Kleine 2017), potentially suggesting a decoupling of stellar sources between these two groups of elements (i.e., Akram *et al.* 2013). Moreover, the low-abundance isotope ^{190}Pt is a *p*-process, or proton-rich, isotope. These form in supernova environments and can yield information on the addition of supernovae components to the solar system (Table 1). To date, however, very few published data exist for ^{190}Pt (Peters *et al.* 2015).

For GCR and nucleosynthetic studies, the combined determination of Pt isotopes with those of other elements, such as Pd, on the same sample aliquot is very beneficial. For example, these combined analyses are crucial to determine whether the nucleosynthetic decoupling of light and heavy nuclides is a true feature and not an artefact due to local sample heterogeneity. Similarly, because GCR effects vary with sample depth, correlated Pd and Pt isotope analyses from the same sample aliquot are vital for the interpretation of neutron capture in meteorites (Mayer *et al.* 2015, Ek *et al.* 2017). Only correlated data allow for discrimination between GCR and nucleosynthetic contributions to Pd isotopes in iron meteorites. Additionally, determining the Pt and Pd mass fractions on the same aliquot of a meteorite consumes less of these precious materials.

To be useful, a separation scheme must isolate Pt from Ir nearly quantitatively, because Ir isotopes can tail onto Pt during mass spectrometry (Kruijer *et al.* 2013, Wittig *et al.* 2013, Peters *et al.* 2015). Furthermore, Ir isotopes can generate isobaric interferences on Pt isotopes in the form

of hydrides. It is also vital to eliminate isobaric interferences from Os isotopes. In particular, the high relative abundance of ^{191}Ir (37.3%), ^{190}Os and ^{192}Os (26.26 and 40.78%, respectively; Table 1) renders ^{190}Pt and ^{192}Pt measurement results with low uncertainties impossible if these elements are not removed to an appropriate level.

Current methods for Pt purification either are not optimised for the collection of both Pt and Pd (Kruijer *et al.* 2013, Wittig *et al.* 2013, Creech *et al.* 2014, Peters *et al.* 2015), or do not separate Pt from Ir well enough for accurate isotopic determination (Rehkämper and Halliday 1997). Here, we present a new measurement procedure that allows the extraction of both Pt and Pd from iron meteorites. The further Pd purification and the determination of high-precision Pd isotope amount ratios by multi-collector inductively coupled plasma-mass spectrometry (MC-ICP-MS) are described in a companion study (Ek *et al.* 2017). Here, we focus on Pt isotope determinations and the separation of Pt from Pd, Ir and Os in preparation for measurement by MC-ICP-MS. The bias and precision of our method was verified using IIAB and IVB iron meteorites and a synthetic reference material.

Methods

Reagents and materials

During the course of this study, double Teflon-distilled hydrochloric (HCl) and nitric (HNO_3) acids were used. Concentrated HCl was ~ 9.8 mol l^{-1}, while concentrated HNO_3 was ~ 14.2 mol l^{-1}. Acids were routinely titrated before use. All H_2O used was of high-purity grade (≥ 18.2 MΩ cm). Saturated bromine solutions ('bromine water') were prepared using Merck Millipore Bromine 99.9999% SUPRAPUR®. The bromine solution was first cleaned by repeatedly adding and decanting high-purity water, before producing the final saturated bromine water solution. The Br water solution was freshly mixed prior to each ion-exchange chemistry and used within 24 h. Ascorbic acid from Sigma Aldrich as FLUKA L-ascorbic acid powder (TraceSELECT®), hydrogen peroxide (H_2O_2; 30% *m/m* Suprapur®) from Merck Millipore, perchloric acid (70% *m/m* Suprapur®) from Merck Millipore and FLUKA analytical-grade ethanol absolute (≤ 99.8%) from Sigma Aldrich were also used.

All anion-exchange procedures utilised BioRad AG® 1-X8 (200–400 mesh, chloride form). The resin was batch-cleaned with 5x the resin volume of 0.8 mol l^{-1} HNO_3, followed by the same quantities of 3 mol l^{-1} HNO_3, concentrated HNO_3, 3 mol l^{-1} HNO_3, high-purity water, 4 mol l^{-1} HCl, concentrated HCl and finally 6 mol l^{-1} HCl.

Meteorite materials studied

Two IVB iron meteorites (Santa Clara and Tawallah Valley), plus North Chile (IIAB, our in-house reference material), were analysed. All samples were taken from the meteorite collection housed at ETH Zürich. Iron meteorites were prepared using a CBN blade fitted to a Buehler Isomet™ low-speed saw, operated with ethanol as the cooling fluid. Samples were then abraded with silicon carbide paper to remove any remaining weathering and fusion crust, and to polish cut surfaces. The new measurement procedure was also tested with Fe-Ni powders (Alfa Aesar, Puratronic® 99.999%) doped with additional elements to match an iron meteorite composition, including Pt, Ir and Pd (30 μg g^{-1} each). The synthetic iron meteorites had initial Ir/Pt ratios of 1.0, which models the most extreme ratios expected in iron meteorites (Campbell and Humayun 2005).

Sample digestion

All materials were digested in precleaned Savillex™ PFA beakers in Class 10 (ISO 4) laminar flow hoods within a Class 1000 (ISO 6) clean laboratory environment. Once in the clean laboratory environment, samples were placed in ethanol in the ultrasonic bath for 5 min, before leaching for 5 min in cold 2 mol l^{-1} HCl prior to weighing and digestion. Samples were digested in a 2:1 mix of concentrated HNO_3 and HCl (~ 8 ml g^{-1} of sample) and refluxed on the hot plate for ~ 48 h at 100 °C. They were treated in an ultrasonic bath at least twice during this period. Once dried, all samples were taken up in concentrated HCl and refluxed overnight. At this stage, the solution was clear, indicating that no undigested sample material remained in the beaker.

Ion-exchange chromatography

Pt-Pd separation (first ion-exchange column): The first anion-exchange chemistry (Pt-Pd separation) is based on Method 1 of Rehkämper and Halliday (1997). Up to 0.3 g of sample per column was taken from the digested mass. Each aliquot was refluxed in a 2:1 mix of concentrated HNO_3 and HCl for ~ 48 h at 100–110 °C. Next, the samples were dried and taken up in 10 ml 0.5 mol l^{-1} HCl + 10% Br water. Bromine water is an oxidant that is used throughout the early stages of the first procedure to keep Ir in its oxidised (Ir^{4+}) state (Rehkämper and Halliday 1997). Samples were refluxed in this mixture overnight at 100–110 °C and treated in the ultrasonic bath at least once during this period.

Quartz glass columns with internal diameters of 6 mm were used during this study. The resin was supported by quartz glass wool (5–30 μm fibre thickness). Columns were loaded with 1.25 ml of precleaned AG1-X8 resin. The resin was further cleaned on the column before the separation procedure was carried out (Steps 1–4, Table 2). Prior to the anion separation procedure, the samples were removed from the hot plate and allowed to cool. The resin was preconditioned with 8 ml 0.5 mol l^{-1} HCl + 10% Br water. The samples were then loaded, followed by 12 ml 1 mol l^{-1} HCl + 10% Br water and 5.5 ml of 0.8 mol l^{-1} HNO_3 + 10% Br water (Figure 1a). Next, concentrated HCl was added to remove as much Ru as possible before Pd elution. Palladium was subsequently eluted in 10 ml of 8 mol l^{-1} HNO_3. This step was loaded in five 2 ml increments and performed using acid heated to 80–90 °C to aid efficient Pd elution (Rehkämper and Halliday 1997). Finally, Pt was removed from the column in 14 ml of 13.5 mol l^{-1} HNO_3. A clean-up fraction consisting of 10 ml of concentrated HNO_3 was collected to verify whether Pt and Pd were fully eluted. The Pd fraction was then further processed for high-precision Pd isotope determinations according to Ek *et al.* (2017), while the Pt elution was purified to remove Ir and Os, as described below.

Pt-Ir separation: Two methods for Pt-Ir separation are presented. For both methods, Pt fractions from the first column were evaporated, redissolved in a 2:1 mixture of concentrated HNO_3 and HCl (1.5 ml) and refluxed for 48 h at 100 °C. Samples were then evaporated to dryness, taken up in 2.5 ml 1 mol l^{-1} HCl and refluxed overnight at 120 °C. Precleaned AG1-X8 resin (1 ml) was loaded into the columns and cleaned again (Steps 1–4, Table 3).

Pt-Ir separation: Method 1 (ascorbic acid): Iridium was reduced by adding ascorbic acid before loading the sample onto the column. Prior to loading onto the columns, the samples were removed from the hot plate and allowed to cool before being diluted to 5 ml 0.5 mol l^{-1} HCl–0.1 mol l^{-1} ascorbic acid. Samples were shaken thoroughly and allowed to stand for ~ 30 min before loading. During this time, the columns were preconditioned with 8 ml 0.5 mol l^{-1} HCl. The sample was then loaded onto the resin and matrix elements were eluted with 10 ml of 0.5 mol l^{-1} HCl. Iridium was then stripped from the column using 20 ml 2 mol l^{-1} HCl. Finally, Pt was eluted in 30 ml of 13.5 mol l^{-1} HNO_3 (Table 3; Figure 1b).

Pt-Ir separation: Method 2 (hydrogen peroxide): The breakdown of H_2O_2 to O_2 can act as a weak reducing agent (e.g., Song and Zhang 2008), and this was utilised to reduce Ir in Method 2 (Table 3; Figure 1c). The samples were diluted to 5 ml 0.5 mol l^{-1} HCl and the columns were preconditioned with 8 ml 0.5 mol l^{-1} HCl. After sample loading, the columns were rinsed with 10 ml 0.5 mol l^{-1} HCl and 20 ml 0.5 mol l^{-1} HCl–1% H_2O_2 to reduce the Ir. Iridium was subsequently eluted in 2 mol l^{-1} HCl. Finally, as in Method 1, Pt was collected in 30 ml of 13.5 mol l^{-1} HNO_3. Depending on the initial Ir/Pt ratio of the sample, the ion-exchange column (Method 1 or 2) was repeated to achieve the required separation of these elements.

Total procedural blanks for the entire chemical separation procedure were typically in the range 0.1–0.3 ng of Pt per 0.3 g sample and are therefore negligible (Pt in samples, 6.6–9.0 μg per 0.3 g of iron meteorite sample; Campbell and Humayun 2005, Wasson *et al.* 2007). The blank contribution to Pd after the first column is 0.05–0.4 ng of Pd per 0.3 g sample.

Preparation for mass spectrometry

Isotopic determination: After Ir was adequately separated from Pt, remaining Os was removed from the sample to achieve unbiased isotopic data. This was accomplished through volatilisation of Os by repeated

Table 2.
Platinum–palladium separation procedure (first column procedure)

Step		Acid	Volume (ml)	Elements eluted
1.	Resin cleaning	0.8 mol l^{-1} HNO_3	20	
2.	Resin cleaning	concentrated HCl	10	Pd
3.	Resin cleaning	concentrated HNO_3	25	Pt, Pd and Ir
4.	Reconversion of resin to chloride form	6 mol l^{-1} HCl	40	
5.	Precondition	0.5 mol l^{-1} HCl + 10% Br water	8	
6.	Loading and matrix elution	0.5 mol l^{-1} HCl + 10% Br water	10	Fe, Ni, Co, Cr, W
7.	Matrix elution	1 mol l^{-1} HCl + 10% Br water	12	Fe, Ni, Co, Cr, minor Ru elution.
8.	Matrix elution	0.8 mol l^{-1} HNO_3 + 10% Br water	5.5	Zn, Cd. Limited elution of Ir.
9.	Matrix elution	concentrated HCl	12	Ag, Ru
10.	Pd elution	8 mol l^{-1} HNO_3 (80–90 °C)	10	Pd with Ru and trace Fe, Ni, Cr.
11.	Pt elution	13.5 mol l^{-1} HNO_3	14	Pt with Ir and trace Fe, Ni, Cr.

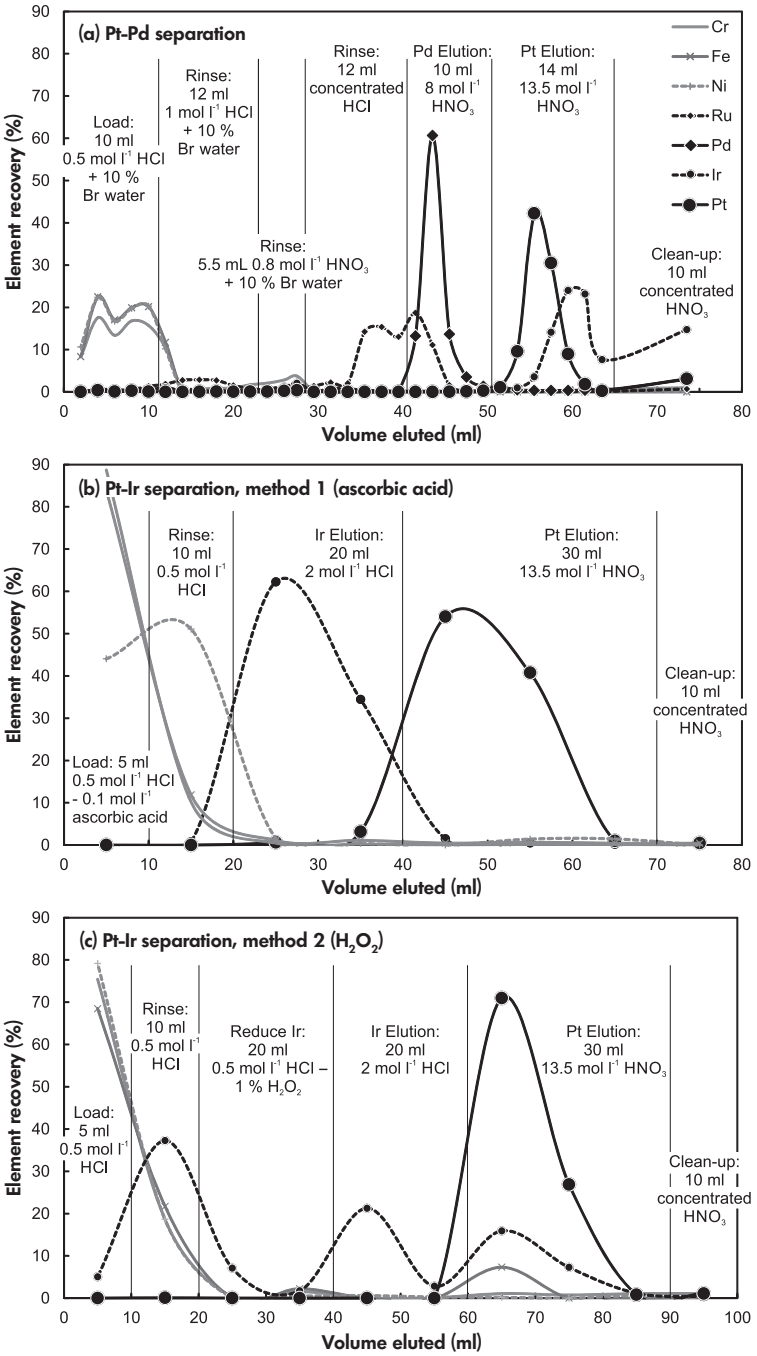

Figure 1. Elution curves for (a) the Pt-Pd separation, (b) the Ir-Pt separation procedure utilising ascorbic acid as a reducing agent (Method 1) and (c) the Ir-Pt separation procedure using H_2O_2 as a reducing agent (Method 2). Elution curves were produced using a synthetic sample with a composition based on an iron meteorite. The starting Ir/Pt ratio for the Pt-Pd separation was 1.0. Both Ir-Pt separation procedures used a starting composition with an Ir/Pt ratio of 0.77, which is based on the Pt fraction eluted during the Pt-Pd separation.

drying with $HClO_4$ (Kruijer *et al.* 2013, Peters *et al.* 2015). To this end, Pt fractions were dried and then taken up in 0.5 ml of 2:1 HNO_3 and HCl. Samples were refluxed overnight at 100 °C and then cooled. Next, 50 µl $HClO_4$ was added to each beaker and the samples were dried. During drying, the temperature was increased incrementally to ~ 205 °C, and held there until all $HClO_4$ was evaporated. This procedure was repeated until the desired Os/Pt was reached, typically three to four times. After treatment with $HClO_4$, the sample was refluxed overnight in

Table 3.
Platinum–iridium separation procedures (Methods 1 and 2; second column procedure)

Step		Acid	Volume (ml)	Elements eluted
1.	Resin cleaning	0.8 mol l^{-1} HNO_3	20	
2.	Resin cleaning	concentrated HCl	10	Pd
3.	Resin cleaning	concentrated HNO_3	25	Pt, Pd and Ir
4.	Reconversion of resin to chloride form	6 mol l^{-1} HCl	40	
Method 1				
5.	Precondition	0.5 mol l^{-1} HCl	8	
6.	Load	0.5 mol l^{-1} HCl–0.1 mol l^{-1} ascorbic acid	5	Fe, Ni
7.	Rinse	0.5 mol l^{-1} HCl	10	Cr, Ni, Fe
8.	Ir elution	2 mol l^{-1} HCl	20	Ir
9.	Pt elution	13.5 mol l^{-1} HNO_3	30	Pt with minor Ir
Method 2				
5.	Precondition	0.5 mol l^{-1} HCl	8	
6.	Load	0.5 mol l^{-1} HCl	5	Fe, Ni
7.	Rinse	0.5 mol l^{-1} HCl	10	Cr, Ni, Fe
8.	Reduce Ir	0.5 mol l^{-1} HCl–1% H_2O_2	20	
9.	Ir elution	2 mol l^{-1} HCl	20	Ir
10.	Pt elution	13.5 mol l^{-1} HNO_3	30	Pt with minor Ir

0.5 ml of 2:1 HNO_3 and HCl and then dried, before being briefly redissolved in 0.5 ml of 5 mol l^{-1} HNO_3 and dried again. Finally, samples were taken up in 5 mol l^{-1} HNO_3 and diluted to 0.5 mol l^{-1} HNO_3 before isotopic determination.

Mass fraction measurements: Samples for mass fraction determinations were evaporated to dryness after column chemistry. They were then refluxed and dried with 0.5 ml *aqua regia*, followed by 0.5 ml HNO_3. Finally, samples were taken up in 5 mol l^{-1} HNO_3 and refluxed overnight, before being diluted to 0.5 mol l^{-1} HNO_3 for analysis.

Mass spectrometry

Isotope ratio measurements: Platinum isotope ratio determinations were performed at ETH Zürich using a Thermo Scientific Neptune *Plus* instrument fitted with a Cetac Aridus II desolvating nebuliser and conventional *H* cones. The machine was operated in low-resolution mode. All Pt isotopes were collected simultaneously, along with $^{188}Os^+$ and $^{200}Hg^+$ to apply corrections for isobaric interferences, and $^{191}Ir^+$ in order to assess Ir tailing effects onto Pt isotopes (Table 4). Two 10^{12} Ω resistors were employed for collecting $^{188}Os^+$ and $^{190}Pt^+$. All other isotopes were collected with 10^{11} Ω resistors.

Detector gain was determined daily before each measurement session. An on-peak baseline (OPB) was collected before each measurement. The OPB was measured as a reference, but was not subtracted during the data reduction described here (see discussion below). For samples and reference solutions, each measurement included a peak centre and a 30-s electronic baseline before sixty integrations of 8.4 s. Samples were bracketed by the NIST SRM 3140 Pt reference solution, and the ion beam intensity of sample and bracketing solution was matched to better than 10%. Between each sample and bracketing solution, 0.5 mol l^{-1} HNO_3 was introduced to reduce the Pt background of the sample introduction system.

Table 4.
Cup configuration used for Pt isotope measurements on the Neptune *Plus* instrument

Cup	L4	L3	L2	L1	C	H1	H2	H3	H4
Isotope	^{188}Os	^{190}Pt	^{191}Ir	^{192}Pt	^{194}Pt	^{195}Pt	^{196}Pt	^{198}Pt	^{200}Hg
Resistor	10^{12}	10^{12}	10^{11}	10^{11}	10^{11}	10^{11}	10^{11}	10^{11}	10^{11}

Resistor values in Ω.

Samples and bracketing solutions were diluted to give a ~ 2×10^{-10} A ion beam for $^{194}Pt^+$. This equates to ~ 300 ng g^{-1} Pt and indicates a sensitivity of ~ 200 V per μg g^{-1} for Pt. Each analysis consumed 0.9–1.2 ml of solution using a nebuliser with an uptake rate of ~ 100 μl min^{-1}, therefore requiring ~ 300 ng Pt per analysis.

Measurement results were corrected for instrumental mass bias using the exponential law and were internally normalised to $^{198}Pt/^{195}Pt$ ('8/5') = 0.2145 (Kruijer *et al.*

2013). Mercury interferences were first corrected on $^{198}Pt^{+}$ using $^{200}Hg/^{198}Hg = 2.31695$ (Berglund and Wieser 2011). The corrected $^{198}Pt^{+}$ was then used for the internal normalisation and interference corrections. The intensity of $^{196}Hg^{+}$ was also stripped off $^{196}Pt^{+}$. The Os interference on $^{192}Pt^{+}$ was corrected using $^{188}Os/^{192}Os = 0.32467$ (Berglund and Wieser 2011). Finally, a 2*s* rejection criterion was applied to the sixty corrected cycles. All data are presented in the epsilon notation (i.e., $\varepsilon^{19i}Pt/^{195}Pt$ = deviation in parts per 10000 from the average of the two bracketing solutions).

Mass fraction measurements: Eluates from the column calibration were analysed using either a Thermo Scientific Element XR (Pt-Pd separation, Ir-Pt separation Method 2) or a Perkin Elmer Elan DRC-e ICP quadrupole mass spectrometer (Ir-Pt separation Method 1) at ETH Zürich. The Thermo Scientific Element XR was operated with conventional *H* cones and a wet plasma introduction system. Platinum-group elements were determined in low-resolution mode; other elements (including Cr, Fe and Ni) were measured in medium resolution. The PerkinElmer Elan DRC-e ICP was operated using a Scott spray chamber. In both cases, analyses were calibrated using synthetic calibration solutions. The measurement precision of both techniques was better than 5% (2 RSD).

Results and discussion

Ion-exchange chemistry

Pt-Pd separation: The first ion-exchange column separated Pt and Pd from each other and removed the majority of matrix elements (Figure 1a; Table 2). Platinum yields from iron meteorites after this column were variable and ranged from 50 to 90%, but were typically 70–90%. Low yields were a result of early Pt elution into the Pd fraction, or Pt not adsorbing to the resin during loading. An additional clean-up fraction of 10 ml concentrated HNO_3 was routinely collected at the end of the column procedure and these fractions contained only 1% of the Pt load. Yields for Pd from iron meteorites after the first column were usually ~ 70–80%, but could be as low as 50%. Palladium often showed peak tailing into the Pt elution, which reduced the Pd yields. Up to 20% of the Pd was eluted with Pt, and a further 8% was routinely present in the clean-up fraction. Tests with synthetic meteorites (Fe and Ni powders doped with PGE RMs) always yielded close to 100% for both Pt and Pd. This suggests that the oxidation state of both Pt and Pd before the column chemistry is important for the yield. Therefore, samples were refluxed in inverse *aqua regia* for ~ 48 h before each column stage to try to fully oxidise these elements and ensure that Pt and Pd were adsorbed to the resin during loading.

The volumes of the sample loading and first elution steps (Steps 6–7, Table 2) were greater than those suggested by Rehkämper and Halliday (1997). Those authors utilised a sulfide fire assay technique to preconcentrate the PGEs, which removes the majority of the Fe matrix. This technique, however, results in relatively high blanks and variable yields for both Pt and Pd (Rehkämper and Halliday 1997, Gros *et al.* 2002, Ren *et al.* 2016). Furthermore, iron meteorites can be readily dissolved using a hot plate digestion, and therefore, that method was chosen for this study. As a result, more matrix elements were loaded on to our columns, and larger acid volumes were necessary to remove these elements (Table 2). Additionally, the samples were loaded in 10 ml 0.5 mol l^{-1} HCl–10% Br_2 (instead of 5–10 ml 1.0 mol l^{-1} HCl–10% Br_2; Rehkämper and Halliday 1997) because the partition coefficient for Fe on strong anion-exchange resin decreases with decreasing HCl concentration, while those for Pt and Pd increase (Kraus and Nelson 1956). Hence, lowering the acid concentration improves the separation of these elements.

Iridium and Pt were not well separated after this first stage of ion-exchange chemistry. Iridium elution in the Pt fraction was ~ 60–80% of the total Ir (with Ir/Pt ranging from ~ 0.2 to 0.8). The poor separation of Ir from Pt is partly due to the use of bromine water. Bromine water acts to keep Ir oxidised and thus retained by the column until rinsed with concentrated HNO_3 (Rehkämper and Halliday 1997). Without the use of bromine water, the fraction of Ir eluted with Pt is ~ 10% lower. Bromine water, however, aids in the elution of Pd by narrowing the Pd elution peak and reducing some of the tailing problems associated with this element, increasing the Pd yield by up to 10%.

Pt-Ir separation: For the further purification of Pt from Ir, a second ion-exchange column was developed. Accurate Pt isotope analyses by MC-ICP-MS rely on low Ir contents in the analysed Pt fraction. This is achieved by utilising the weak affinity of Ir^{3+} for strong anion resin (Kraus and Nelson 1956). Once Ir^{4+} has been reduced to Ir^{3+}, it can be efficiently eluted from the column with HCl before Pt (Anbar *et al.* 1997, Pearson and Woodland 2000). Sulfurous acid and ascorbic acid were used previously for Ir reduction (Anbar *et al.* 1997, Wittig *et al.* 2013). We tested ascorbic acid (Method 1; Figure 1b) and H_2O_2 (Method 2; Figure 1c). Iridium elution in the Pt fraction can be decreased to between 2–15% of the total Ir using ascorbic acid as a reducing agent, and to ~ 25% when using H_2O_2. These results indicate that ascorbic acid is the more effective reducing agent, while in both cases, 70–100% of the Pt is

retained. Yields for Pt for the full ion-exchange column were 50–70%. In both Methods 1 and 2, the column was rinsed with 0.5 mol l^{-1} HCl after the sample was loaded, which eluted remaining matrix elements to the extent that they were absent or insignificant during MC-ICP-MS analysis. Method 1 (ascorbic reduction) was chosen as our primary technique because of the better Ir removal. Therefore, all samples and reference materials for isotope determination were processed following this procedure.

Os volatilisation: Osmium was near-quantitatively removed during the two-stage ion-exchange procedure. However, a final stage of evaporation in a mixture of inverse *aqua regia* and perchloric acid at ≥ 180 °C was necessary to allow precise ε^{192}Pt measurements. This procedure was typically repeated three to four times until $^{188}Os^{+}/^{195}Pt^{+} < 3 \times 10^{-5}$ (see discussion of this value below). An additional benefit of drying the samples in $HClO_4$ is the destruction of organic molecules. These result from the use of (i) high molarity HNO_3, which can attack and release the organics from the resin (e.g., Schönbächler and Fehr 2014), and (ii) ascorbic acid.

High-precision Pt isotope measurements

Interferences in the mass spectrum and corrections: Doping tests were performed to determine the level of interfering ions that could be tolerated for measurement results with low uncertainties. $^{192}Os^{+}$ can create a significant interference on $^{192}Pt^{+}$ intensities, thus having an effect on ε^{192}Pt, and must be removed so that $^{188}Os^{+}/^{195}Pt^{+} < 3 \times 10^{-5}$ (Figure 2). Below this level, doping tests show that an accurate correction for the isobaric interference from $^{192}Os^{+}$ on $^{192}Pt^{+}$ is possible. For a $^{188}Os^{+}/^{195}Pt^{+}$ ratio of 3×10^{-5}, the correction to ε^{192}Pt is ~41 ε. The $^{188}Os^{+}/^{195}Pt^{+}$ ratio of the IVB iron meteorites after the chemical separation procedure was always significantly lower and required Os corrections to ε^{192}Pt in the range of 1.3–3.1 ε.

Mercury ion intensities were not detected above background level in any sample, although Hg can be present in the Ar gas used by the mass spectrometer (e.g., Thirlwall 2002). A minor correction for Hg was applied by peak stripping during the data reduction process (correction to $\varepsilon^{196}Pt < 0.02$; see the 'Mass Spectrometry' section). In addition, an OPB was determined before each measurement of a sample or bracketing solution to subtract background Hg. Data were processed both with and without the subtraction of this OPB. This correction did not result in an improvement to ratios where Hg interferences were present, because background Hg levels were extremely low ($^{200}Hg^{+} < 0.1$ mV). At the same time,

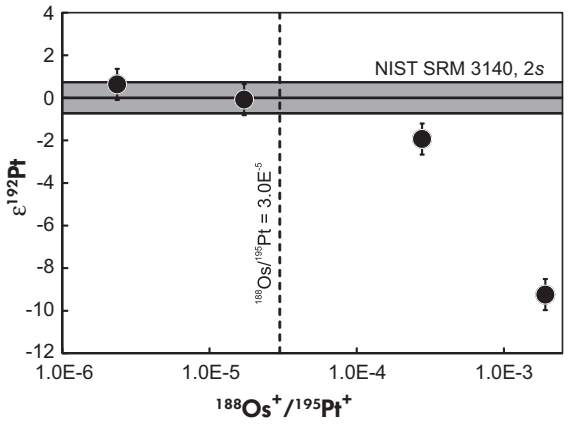

Figure 2. The $^{188}Os^{+}/^{195}Pt^{+}$ ratios relative to ε^{192}Pt for standard solutions doped with Os. Platinum ratios are corrected for Os interferences. The results indicate that the $^{188}Os^{+}/^{195}Pt^{+}$ ratio must be below 3×10^{-5} to obtain accurate Pt isotope data. The grey bar represents the short-term (daily) 2*s* precision of the Pt bracketing solution NIST SRM 3140. Individual measurement precisions are based on the 2*s* value obtained from repeat analyses of the North Chile in-house reference material (Table 5).

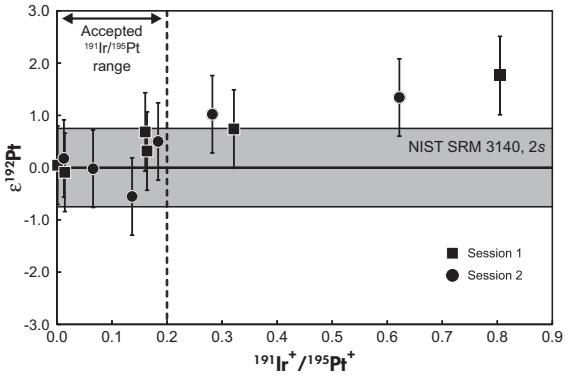

Figure 3. The $^{191}Ir^{+}/^{195}Pt^{+}$ ratios relative to ε^{192}Pt for standard solutions doped with Ir. Iridium causes tailing on Pt isotopes. The results from two measurement sessions indicate that these effects are negligible for samples with $^{191}Ir^{+}/^{195}Pt^{+}$ ratios of < 0.2. After processing through our new ion-exchange procedure, natural samples analysed as part of this study showed very low $^{191}Ir^{+}/^{195}Pt^{+}$ ratios of between 0.01 and 0.06. The grey bar represents the short-term (daily) 2*s* precision of the Pt bracketing solution NIST SRM 3140. Individual measurement repeatability as in Figure 2.

background Os is negligible but small variations in the OPB measurements resulted in inaccuracies to the Os correction applied to $^{192}Pt^{+}$ when the OPB was subtracted. The subtraction of the OPB increased the scatter (2 standard deviations, 2*s*) of $\varepsilon^{192}Pt$ from ~ 0.75 to ~ 0.90 for the Pt bracketing solution NIST SRM 3140. For this reason, the data presented here were not corrected with the OPB.

Tailing from Ir isotopes onto Pt isotopes also presents a significant challenge during Pt isotope determination. This is because the high-abundance isotopes $^{191}Ir^{+}$ (37.3%) and $^{193}Ir^{+}$ (62.7%) produce tailing on the adjacent $^{192}Pt^{+}$ peak (0.78%) (Kruijer *et al.* 2013, Wittig *et al.* 2013, Peters *et al.* 2015). This results in a perceived excess of $^{192}Pt^{+}$. To a lesser degree, this effect is also present on $^{194}Pt^{+}$ (32.86%). Additionally, Ir can generate hydride interferences on Pt isotopes, which is less of a concern for this study because the samples were analysed with a desolvating nebuliser. Tests using Pt standard solutions doped with various amounts of Ir demonstrate the combined effect of Ir tailing and hydride formation on $\varepsilon^{192}Pt$ (Figure 3). For $^{191}Ir^{+}/^{195}Pt^{+}$ ratios of 0.28 or more, excesses of at least 1 ε can be induced on $\varepsilon^{192}Pt$. Furthermore, the addition of Ir suppresses the Pt signal. To ensure that no corrections for Ir tailing were necessary, samples were passed through the second ion-exchange column until a $^{191}Ir^{+}/^{195}Pt^{+}$ ratio of < 0.2 (equivalent to an Ir/Pt ratio of < 0.13) was achieved. For samples with initial elemental Ir/Pt ratios of < 0.5, this was usually achieved after a single column pass. After two repeats, all samples displayed $^{191}Ir^{+}/^{195}Pt^{+}$ ratios < 0.2, and usually lower than 0.1. However, care must be taken as the magnitude of Ir tailing can vary between measurement sessions with instrument settings. Pressure in the back-end of the mass spectrometer should also be monitored carefully and additional doping tests performed as necessary, particularly for samples that are close to the $^{191}Ir^{+}/^{195}Pt^{+}$ threshold.

Table 5.
Platinum isotope data for the North Chile meteorite

	Yield[a]	$\varepsilon^{192}Pt$	2SE[b]	$\varepsilon^{194}Pt$	2SE[b]	$\varepsilon^{196}Pt$	2SE[b]
North Chile A	59%						
10.03.2015		1.45	0.22	0.35	0.04	0.18	0.04
10.03.2015		1.29	0.21	0.30	0.04	0.18	0.04
07.05.2015		1.36	0.19	0.36	0.05	0.23	0.04
07.05.2015		0.71	0.19	0.36	0.05	0.21	0.04
08.05.2015		0.73	0.20	0.28	0.04	0.20	0.04
08.05.2015		1.12	0.18	0.35	0.03	0.20	0.03
15.12.2015		1.06	0.22	0.34	0.04	0.24	0.03
15.12.2015		0.67	0.18	0.35	0.04	0.17	0.03
15.12.2015		1.31	0.19	0.32	0.04	0.20	0.03
16.12.2015		0.54	0.18	0.36	0.04	0.21	0.03
Mean (*n* = 10)		1.02		0.34		0.20	
2*s*		0.67		0.06		0.04	
North Chile B	51%						
07.05.2015		0.79	0.13	0.13	0.04	0.09	0.03
07.05.2015		1.34	0.14	0.14	0.04	0.07	0.03
Mean (*n* = 2)		1.07		0.14		0.08	
North Chile C	68%						
15.12.2015		1.27	0.19	0.27	0.05	0.15	0.03
15.12.2015		0.22	0.17	0.24	0.04	0.18	0.04
15.12.2015		0.57	0.20	0.26	0.04	0.18	0.04
16.12.2015		1.01	0.17	0.22	0.04	0.12	0.03
16.12.2015		1.23	0.18	0.25	0.05	0.17	0.04
16.12.2015		1.50	0.21	0.19	0.04	0.15	0.03
Mean (*n* = 6)		0.97		0.24		0.16	
2*s*		0.96		0.06		0.05	
North Chile D	69%						
29.06.2016		0.82	0.18	0.23	0.06	0.15	0.04
Precision based on North Chile A, B, C and D:							
Mean (*n* = 19)		1.00		0.28		0.17	
2*s*		0.73		0.15		0.09	

[a] Yield after column chemistry for each aliquot of North Chile. [b] Precision of measured $\varepsilon^{191}Pt$ values is given as 2 standard errors of the single measurements.

Other major molecular interferences on Pt isotope ions in the mass spectrum of meteorite samples may arise from W (WC^+, WN^+, WO^+) or Au (AuH^+). Our new ion-exchange procedure essentially completely removes these elements. Occasionally, trace levels of W were detected in the samples ($^{183}W^+/^{195}Pt^+$ up to a maximum of 0.0003). However, W doping tests up to a $^{183}W^+/^{195}Pt^+$ ratio of 0.0035 exhibited no offsets to any Pt isotope ratios. Iron and Ni are present at background levels in samples and are important to monitor. Nickel doping tests were conducted as part of this study and indicate that at high levels of Ni ($^{60}Ni^+/^{195}Pt^+ > 0.067$), a deficit of -0.6 on $\varepsilon^{192}Pt$ can be induced. However, this effect is not significant for our current study, where the $^{60}Ni^+/^{195}Pt^+$ ratio was < 0.024 in all samples analysed.

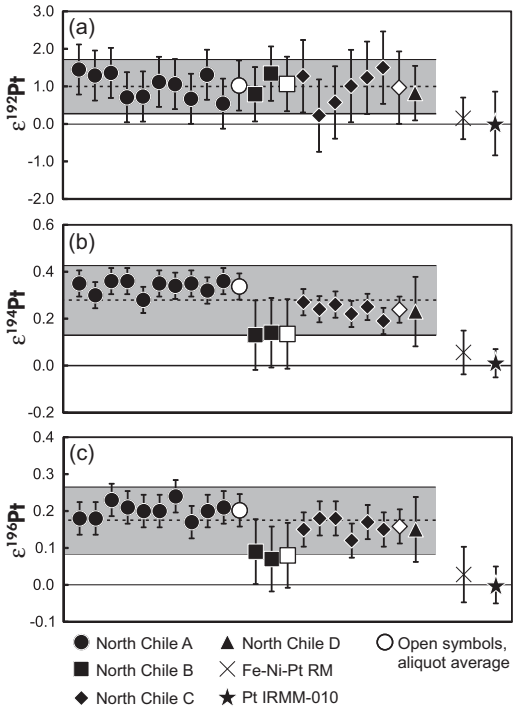

Figure 4. The Pt isotope composition of four different aliquots from North Chile, an Fe-Ni powder doped with NIST SRM 3140, and the pure Pt reference material IRMM-010: (a) $\varepsilon^{192}Pt$, (b) $\varepsilon^{194}Pt$ and (c) $\varepsilon^{196}Pt$. The averages for the Fe-Ni-Pt RM passed through our column procedure and IRMM-010 both yielded ratios that were within precision of the terrestrial value. The dashed line and grey band represent the mean and 2*s* of all nineteen measurements of the North Chile material. Open symbols represent the average of each aliquot. Intermediate precision values (2*s*) for North Chile A and C are based on those aliquots (individual measurements and aliquot average; Table 5). Precisions (2*s*) for the Fe-Ni-Pt RM and IRMM-010 were calculated using those data sets (Table 6). All other precisions are based on the overall 2*s* intermediate precision value of the North Chile sample (*n* = 19).

Measurement precision and bias estimates of Pt isotope measurements: The precision of measured $\varepsilon^{191}Pt$ values is given as 2 standard errors (2SE) of the single measurements (Tables 5, 6 and 7). The typical daily repeatability precision expressed as 2*s* of the Pt bracketing solution NIST SRM 3140 was ~ 0.75 for $\varepsilon^{192}Pt$ and 0.05–0.07 for both $\varepsilon^{194}Pt$ and $\varepsilon^{196}Pt$. A more robust assessment of the precision that includes the entire measurement procedure (from digestion to measurement) is given by repeated analysis of the IIAB iron meteorite North Chile, which was used as an in-house reference material. Approximately 3 g of this sample was dissolved and four 0.3 g aliquots were independently passed through our chemical separation procedure. Nineteen measurements of this RM were performed over the course of six measurement sessions (Table 5 and Figure 4). As this is a natural, nonterrestrial material, Pt isotope ratios are not expected to be within a precision of 0 (see discussion below); however, North Chile can be used to assess the precision of our technique. The precision, expressed as 2*s*, obtained for all four aliquots was 0.73 for $\varepsilon^{192}Pt$, 0.15 for $\varepsilon^{194}Pt$ and 0.09 for $\varepsilon^{196}Pt$ (n = 19). The intermediate precision (2*s*) for a single aliquot (North Chile A) analysed over five sessions was better, yielding 0.67 for $\varepsilon^{192}Pt$, 0.06 for $\varepsilon^{194}Pt$ and 0.04 for $\varepsilon^{196}Pt$ (n = 10). These data show that replicate analyses of samples processed through the entire measurement procedure yield a larger variance (expressed as 2*s*), particularly on $\varepsilon^{194}Pt$, compared with replicate analyses of a single sample solution. This is likely due to the small, but variable, amount of matrix elements that remains in the purified sample solution after the ion-exchange chemistry. Matrix elements remaining in Pt fractions for iron meteorites can include Ni (1–8 ng per sample), Pd (up to 40 ng) and Fe (1–5 ng per sample). Minor organic interferences may also remain from the use of ascorbic acid and from the ion-exchange resin. Values for the overall precision on $\varepsilon^{194}Pt$ and $\varepsilon^{196}Pt$ are similar to previous studies when comparing analyses with similar signal intensities (Kruijer *et al.* 2013, 2014, Wittig *et al.* 2013), although our precision for $\varepsilon^{192}Pt$ is significantly improved compared with Kruijer *et al.* (2013, 2014) due to the lack of an Ir tailing correction required in our study.

To test the accuracy of our method, iron-nickel powders were doped with NIST SRM 3140 and passed through our column procedure. This yielded results that are within a precision of 0 for all ratios (Table 6; Figure 4), indicating that our new procedure is bias free within the limits of our

precision values. Additionally, the Pt reference material IRMM-010 was analysed relative to the NIST SRM 3140 reference solution (Table 6; Figure 4). The results were identical within uncertainty to the NIST SRM 3140 reference solution for all ratios (0.01 ± 0.85 for ε^{192}Pt, 0.01 ± 0.06 for ε^{194}Pt and 0.00 ± 0.05 for ε^{196}Pt; precisions are 2*s*, n = 10).

Although the chemical purification procedure described here can also be used for the measurement of the $^{190}Pt^{+}$ signal (0.012%), a different MC-ICP-MS set-up was necessary to perform these challenging measurements. Therefore, results for ε^{190}Pt are not discussed further in this contribution.

IVB iron meteorites

The Pt isotope compositions for the IVB irons Santa Clara and Tawallah Valley showed positive offsets relative to the terrestrial reference material for all three ratios (Table 7). In particular, ε^{192}Pt varied between the two samples, with ε^{192}Pt of 15.36 ± 0.71 for Santa Clara and 7.37 ± 0.32 for Tawallah Valley. Platinum isotope differences between samples from the same iron meteorite groups have been attributed to the effects of GCR irradiation in space (Kruijer *et al.* 2013, 2014, Wittig *et al.* 2013). For example, neutron capture by ^{195}Pt creates excess ^{196}Pt. Furthermore, the magnitude of the offsets induced by GCR irradiation is related to both exposure time in space and the depth of a sample below the surface of a meteoroid (Leya and Masarik 2013). Large effects are also generated on ε^{192}Pt, because ^{191}Ir captures a neutron and subsequently β-decays to ^{192}Pt (Leya and Masarik 2013). A similar reaction creates ^{194}Pt from ^{193}Ir. The Ir/Pt ratio of a sample is therefore important, particularly to the amount of ^{192}Pt produced (Figure 5a). North Chile has an Ir/Pt ratio of 0.16 (Wasson *et al.* 2007), and Pt isotope data fit well to GCR trends modelled with this value (Figure 5). The Ir/Pt ratios of the IVBs are 0.73 ± 0.05 for Santa Clara and 0.57 ± 0.04 for Tawallah Valley (ratios and 1*s* uncertainties calculated from Campbell and Humayun 2005, these uncertainties are represented by grey areas in Figure 5). Data for the IVBs, shown with those from previous studies for the same meteorites, fall within uncertainty of the modelled neutron capture trends for the stated Ir/Pt ratios (Leya and Masarik 2013, Figure 5), and this supports the conclusion that Pt isotopes vary in iron meteorites as a result of exposure to GCR.

Both Tawallah Valley and Santa Clara were sampled from a similar location in the meteorite as by Kruijer *et al.* (2013). Results from the two studies overlap for ε^{194}Pt and ε^{196}Pt for both samples, within uncertainty (Figure 5b). However, our new ε^{192}Pt data for Santa Clara do not

Table 6.
Platinum isotope data for the Pt reference material IRMM-010 and an Fe-Ni powder mixture doped with Pt NIST SRM 3140 and passed through the column procedure described in this study

	ε^{192}Pt	2SE[a]	ε^{194}Pt	2SE[a]	ε^{196}Pt	2SE[a]
Fe-Ni-Pt RM						
Fe-Ni-Pt RM 01	0.54	0.13	0.11	0.05	0.09	0.04
Fe-Ni-Pt RM 02	-0.09	0.12	0.08	0.03	0.02	0.03
Fe-Ni-Pt RM 03	-0.14	0.17	0.03	0.06	0.01	0.04
Fe-Ni-Pt RM 04	0.27	0.15	-0.01	0.05	-0.01	0.03
Fe-Ni-Pt RM 05	0.16	0.20	0.07	0.05	0.03	0.04
Mean	0.15		0.06		0.03	
2*s*	0.56		0.09		0.08	
IRMM-010						
IRMM-010-01	-0.60	0.25	-0.02	0.05	0.00	0.03
IRMM-010-02	0.09	0.21	0.04	0.05	0.03	0.04
IRMM-010-03	-0.01	0.17	0.03	0.05	-0.04	0.04
IRMM-010-04	-0.45	0.22	-0.03	0.05	-0.03	0.04
IRMM-010-05	0.82	0.25	0.04	0.04	0.02	0.04
IRMM-010-06	0.35	0.18	-0.01	0.06	0.00	0.04
IRMM-010-07	0.35	0.19	0.05	0.06	-0.04	0.04
IRMM-010-08	0.08	0.19	-0.01	0.05	-0.01	0.03
IRMM-010-09	-0.25	0.25	0.05	0.05	0.02	0.04
IRMM-010-10	-0.24	0.23	-0.01	0.04	0.02	0.03
IRMM-010 Mean	0.01		0.01		0.00	
2*s*	0.85		0.06		0.05	

[a] Precision of measured ε^{191}Pt values is given as 2 standard errors of the single measurements

agree well with Kruijer *et al.* (2013; Figure 5a), with a difference of at least 3.5 ε between the two data sets. There are two possible reasons for this. First, the data set of Kruijer *et al.* (2013) is subject to large corrections for peak tailing of Ir onto Pt. These authors state that corrections of between ~ 2 and 15 ε were applied to ε^{192}Pt, while the size of the correction to individual samples is not given. Kruijer *et al.* (2013) estimate their ε^{192}Pt uncertainty after peak tailing correction to 2.2 ε; nevertheless, the need to apply such large corrections may have contributed to the discrepancy between our two data sets. Second, GCR-induced effects change with sample depth and hence across a sample on a cm scale (i.e., at the hand-specimen size). In a meteoroid with a pre-atmospheric radius of 60 cm and Ir/Pt = 0.73, the isotopic shift on ε^{192}Pt is predicted to be as much as 1.2 ε per cm in the outer portions of the body (Leya and Masarik 2013). Thus, a difference of ~ 3 cm between sampling locations may be enough to generate the discrepancy observed on ε^{192}Pt. Additionally, because of the smaller shifts induced on ε^{194}Pt and ε^{196}Pt, no concomitant effects would be detectable for these isotopes at the level of uncertainty.

The samples analysed here were also measured by Wittig *et al.* (2013; Figure 5). It is not known how our sampling locations relate to theirs and we make comparisons with caution. Our results for Tawallah Valley and Santa Clara agree well for the ε^{192}Pt and ε^{194}Pt data, given the expected GCR variations on a local scale. However, our ε^{196}Pt values are consistently ~ 0.4 ε higher than those from Wittig *et al.* (2013; Figure 5). Since our ε^{196}Pt data correlate well with ε^{192}Pt, fit the predictions of Leya and Masarik (2013) well and are in good agreement with those of Kruijer *et al.* (2013), we are confident that our values are representative of the samples analysed.

Conclusions

This study presents a new measurement procedure for the separation of Pt and Pd from iron meteorite samples and the determination of Pt isotope amount ratios by MC-ICP-MS. The method was tested using three iron meteorite samples and a terrestrial reference material. After dissolution, a two-stage column procedure utilising strong anion resin was employed. In the first stage, Pt was separated from major matrix constituents, including Fe and Ni. This stage also allowed the isolation and collection of Pd, which can yield information complimentary to Pt for a range of geological questions. The second stage separated Pt from Ir, which can cause peak tailing interferences during mass spectrometry. Reduction of Ir with ascorbic acid before the column procedure exploits the weak affinity of Ir^{3+} for strong anion exchangers, and allowed separation of Pt from Ir. Finally, Os, which generates isobaric interferences on Pt isotopes in the mass spectrum, could be volatilised using perchloric acid. Platinum yields for this procedure were typically 50–70%, and blanks were in the range of 0.1–0.3 ng per 0.3 g test portion.

Table 7.
Platinum isotope amount ratios for the IVB iron meteorites Santa Clara and Tawallah Valley

		Date	ε^{192}Pt	2SE[a]	ε^{194}Pt	2SE[a]	ε^{196}Pt	2SE[a]
Santa Clara								
Santa Clara	01	01.09.14	15.95	0.19	0.65	0.05	0.36	0.03
Santa Clara	02	01.09.14	15.17	0.23	0.52	0.05	0.34	0.04
Santa Clara	03	03.09.14	15.14	0.20	0.70	0.05	0.41	0.03
Santa Clara	04	03.09.14	15.09	0.21	0.70	0.06	0.40	0.04
Santa Clara	05[b]	29.06.16	15.44	0.20	0.60	0.04	0.38	0.03
Santa Clara mean (n = 5)			15.36		0.63		0.38	
2s			0.71		0.15		0.06	
Tawallah Valley								
Tawallah Valley	01	01.09.14	7.33	0.19	0.41	0.05	0.25	0.04
Tawallah Valley	02	03.09.14	7.16	0.21	0.25	0.05	0.22	0.05
Tawallah Valley	03	03.09.14	7.41	0.18	0.34	0.05	0.19	0.03
Tawallah Valley	04	03.09.14	7.32	0.19	0.46	0.05	0.27	0.04
Tawallah Valley	05[b]	12.11.16	7.60	0.15	0.37	0.04	0.27	0.04
Tawallah Valley mean (n = 5)			7.37		0.36		0.24	
2s			0.32		0.16		0.07	

[a] Precision of measured ε^{191}Pt values is given as 2 standard errors of the single measurements. [b] Data obtained on a different aliquot of the same digestion solution processed over the separation procedure.

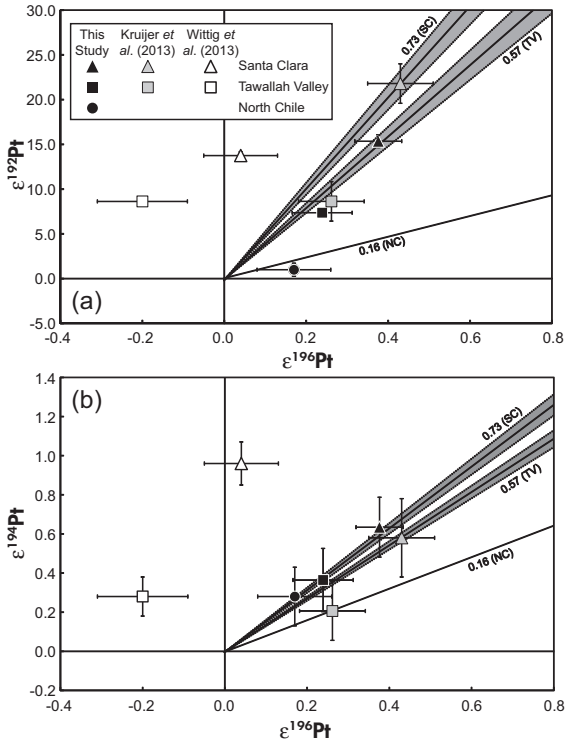

Figure 5. The ε^{192}Pt (a) and ε^{194}Pt (b) isotope composition shown relative to ε^{196}Pt for the IVB iron meteorites Santa Clara (SC) and Tawallah Valley (TV), and the IIAB North Chile (NC). Data from other studies for the same IVB meteorites are from Kruijer *et al.* (2013) and Wittig *et al.* (2013). The solid lines illustrate the expected GCR trends from Leya and Masarik (2013) calculated with an exposure time of 1200 Ma and Ir/Pt suitable for each sample. Numbers on the slopes show the Ir/Pt ratio for the respective meteorite: North Chile from Wasson *et al.* (2007); Tawallah Valley and Santa Clara from Campbell and Humayun (2005). The grey bands represent the precision of the measurement results of Campbell and Humayun (2005). Intermediate precisions (this study) are 2*s* values calculated for each sample from repeat analyses.

The precision of our procedure was assessed using the IIAB iron meteorite North Chile. Repeat analyses of multiple aliquots of this material indicated that the precision of the procedure was 0.73 for ε^{192}Pt, 0.15 for ε^{194}Pt and 0.09 for ε^{196}Pt (n = 19). An iron-nickel powder doped with NIST SRM 3140 and passed through the column procedure described in this study yielded results that were within a precision of 0 for all ratios, indicating that the measurement results derived using the new measurement procedure were unbiased within the limits of the determined precisions. Data for the IVB iron meteorites Santa Clara and Tawallah Valley generally compare well with those of Kruijer *et al.* (2013), but ε^{196}Pt values were significantly different than those reported by Wittig *et al.* (2013). The data fit to modelled trends for neutron capture and support that Pt isotope variations in iron meteorites are a result of variable exposure to galactic cosmic ray irradiation.

Acknowledgements

This work was supported by the European Research Council under the European Union's Seventh Framework Programme (FP7/2007–2013)/ERC Grant agreement n° [279779]. We wish to thank David Cook, Manuela Fehr and Thomas Kruijer for their helpful discussions during this study. We also wish to thank the editor and two anonymous reviewers for their comments on this manuscript.

References

Akram W., Schönbächler M., Sprung P. and Vogel N. (2013)
Zirconium–hafnium isotope evidence from meteorites for the decoupled synthesis of light and heavy neutron-rich nuclei. The Astrophysical Journal, 777, 169.

Akram W., Schönbächler M., Bisterzo S. and Gallino R. (2015)
Zirconium isotope evidence for the heterogeneous distribution of *s*-process materials in the solar system. Geochimica et Cosmochimica Acta, 165, 484–500.

Anbar A.D., Papanastassiou D.A. and Wasserburg G.J. (1997)
Determination of iridium in natural waters by clean chemical extraction and negative thermal ionization mass spectrometry. Analytical Chemistry, 69, 2444–2450.

Berglund M. and Wieser M.E. (2011)
Isotopic compositions of the elements 2009 (IUPAC Technical Report). Pure and Applied Chemistry, 83, 397–410.

Bisterzo S., Gallino R., Straniero O., Cristallo S. and Käppeler F. (2011)
The *s*-process in low-metallicity stars – II. Interpretation of high-resolution spectroscopic observations with asymptotic giant branch models. Monthly Notices of the Royal Astronomical Society, 418, 284–319.

references

Burkhardt C., Kleine T., Dauphas N. and Wieler R. (2012)
Origin of isotopic heterogeneity in the solar nebula by thermal processing and mixing of nebular dust. Earth and Planetary Science Letters, 357–358, 298–307.

Campbell A.J. and Humayun M. (2005)
Compositions of group IVB iron meteorites and their parent melt. Geochimica et Cosmochimica Acta, 69, 4733–4744.

Cotton F.A., Wilkinson G., Murillo C.A. and Bochmann M. (1999)
Advanced inorganic chemistry (6th edition). Wiley (New York), 1376pp.

Creech J.B., Baker J.A., Handler M.R., Schiller M. and Bizzarro M. (2013)
Platinum stable isotope ratio measurements by double-spike multiple collector ICP-MS. Journal of Analytical Atomic Spectrometry, 28, 853–865.

Creech J.B., Baker J.A., Handler M.R. and Bizzarro M. (2014)
Platinum stable isotope analysis of geological standard reference materials by double-spike MC-ICP-MS. Chemical Geology, 363, 293–300.

Creech J.B., Baker J.A., Handler M.R., Lorand J.P., Storey M., Wainwright A.N., Luguet A., Moynier F. and Bizzarro M. (2017)
Late accretion history of the terrestrial planets inferred from platinum stable isotopes. Geochemical Perspectives Letters, 3, 94–104.

Dauphas N., Davis A.M., Marty B. and Reisberg L. (2004)
The cosmic molybdenum–ruthenium isotope correlation. Earth and Planetary Science Letters, 226, 465–475.

Ek M., Hunt A.C. and Schonbachler M. (2017)
A new method for high-precision palladium isotope analyses of iron meteorites and other metal samples. Journal of Analytical Atomic Spectrometry, 32, 647–656.

Fischer-Gödde M. and Kleine T. (2017)
Ruthenium isotopic evidence for an inner Solar System origin of the late veneer. Nature, 541, 525–527.

Fischer-Gödde M., Burkhardt C., Kruijer T.S. and Kleine T. (2015)
Ru isotope heterogeneity in the solar protoplanetary disk. Geochimica et Cosmochimica Acta, 168, 151–171.

Gros M., Lorand J.-P. and Luguet A. (2002)
Analysis of platinum-group elements and gold in geological materials using NiS fire assay and Te coprecipitation: The NiS dissolution step revisited. Chemical Geology, 185, 179–190.

Kleine T., Mezger K., Palme H., Scherer E. and Münker C. (2005)
Early core formation in asteroids and late accretion of chondrite parent bodies: Evidence from ^{182}Hf-^{182}W in CAIs, metal-rich chondrites, and iron meteorites. Geochimica et Cosmochimica Acta, 69, 5805–5818.

Kraus K.A. and Nelson F. (1956)
Anion-exchange studies of the fission products. Proceedings of the 1st UN Conference on Peaceful Uses of Atomic Energy, 7, 113–125.

Kruijer T.S., Fischer-Gödde M., Kleine T., Sprung P., Leya I. and Wieler R. (2013)
Neutron capture on Pt isotopes in iron meteorites and the Hf–W chronology of core formation in planetesimals. Earth and Planetary Science Letters, 361, 162–172.

Kruijer T.S., Touboul M., Fischer-Gödde M., Bermingham K.R., Walker R.J. and Kleine T. (2014)
Protracted core formation and rapid accretion of protoplanets. Science, 344, 1150–1154.

Leya I. and Masarik J. (2013)
Thermal neutron capture effects in radioactive and stable nuclide systems. Meteoritics and Planetary Science, 48, 665–685.

Leya I., Wieler R. and Halliday A.N. (2000)
Cosmic-ray production of tungsten isotopes in lunar samples and meteorites and its implications for Hf–W cosmochemistry. Earth and Planetary Science Letters, 175, 1–12.

Lodders K. (2003)
Solar system abundances and condensation temperatures of the elements. The Astrophysical Journal, 591, 1220–1247.

Markowski A., Leya I., Quitté G., Ammon K., Halliday A.N. and Wieler R. (2006)
Correlated helium-3 and tungsten isotopes in iron meteorites: Quantitative cosmogenic corrections and planetesimal formation times. Earth and Planetary Science Letters, 250, 104–115.

Masarik J. (1997)
Contribution of neutron-capture reactions to observed tungsten isotopic ratios. Earth and Planetary Science Letters, 152, 181–185.

Matthes M., Fischer-Gödde M., Kruijer T.S., Leya I. and Kleine T. (2015)
Pd–Ag chronometry of iron meteorites: Correction of neutron capture-effects and application to the cooling history of differentiated protoplanets. Geochimica et Cosmochimica Acta, 169, 45–62.

Mayer B., Wittig N., Humayun M. and Leya I. (2015)
Palladium isotopic evidence for nucleosynthetic and cosmogenic isotope anomalies in IVB iron meteorites. The Astrophysical Journal, 809, 180.

Pearson D.G. and Woodland S.J. (2000)
Solvent extraction/anion exchange separation and determination of PGEs (Os, Ir, Pt, Pd, Ru) and Re-Os isotopes in geological samples by isotope dilution ICP-MS. Chemical Geology, 165, 87–107.

Peters S.T.M., Münker C., Wombacher F. and Elfers B.-M. (2015)
Precise determination of low abundance isotopes (^{174}Hf, ^{180}W and ^{190}Pt) in terrestrial materials and meteorites using multiple collector ICP-MS equipped with 10^{12} Ω Faraday amplifiers. Chemical Geology, 413, 132–145.

references

Rehkämper M. and Halliday A.N. (1997)
Development and application of new ion-exchange techniques for the separation of the platinum-group and other siderophile elements from geological samples. Talanta, 44, 663–672.

Ren M., Sun Y., Wang C.Y. and Sun S. (2016)
Determination of platinum-group elements in geological samples by isotope dilution-inductively coupled plasma-mass spectrometry combined with sulfide fire assay preconcentration. Geostandards and Geoanalytical Research, 40, 67–83.

Schönbächler M. and Fehr M.A. (2014)
Basics of ion exchange chromatography for selected geological applications. In: Holland H.D. and Turekian K.K. (eds), Treatise on Geochemistry (2nd edition). Elsevier (Oxford), 123–146.

Song C. and Zhang J. (2008)
Electrocatalytic oxygen reduction reaction. In: Zhang J. (ed.), PEM fuel cell electrocatalysts and catalyst layers: Fundamentals and applications. Springer (London), 89–134.

Sprung P., Scherer E.E., Upadhyay D., Leya I. and Mezger K. (2010)
Non-nucleosynthetic heterogeneity in non-radiogenic stable Hf isotopes: Implications for early solar system chronology. Earth and Planetary Science Letters, 295, 1–11.

Thirlwall M.F. (2002)
Multicollector ICP-MS analysis of Pb isotopes using a ^{207}Pb-^{204}Pb double spike demonstrates up to 400 ppm/amu systematic errors in Tl-normalization. Chemical Geology, 184, 255–279.

Trinquier A., Elliott T., Ulfbeck D., Coath C., Krot A.N. and Bizzarro M. (2009)
Origin of nucleosynthetic isotope heterogeneity in the solar protoplanetary disk. Science, 324, 374–376.

Vanhala H.A.T. and Boss A.P. (2002)
Injection of radioactivities into the forming solar system. The Astrophysical Journal, 575, 1144.

Walker R.J. (2012)
Evidence for homogeneous distribution of osmium in the protosolar nebula. Earth and Planetary Science Letters, 351–352, 36–44.

Wasson J.T., Huber H. and Malvin D.J. (2007)
Formation of IIAB iron meteorites. Geochimica et Cosmochimica Acta, 71, 760–781.

Wittig N., Humayun M., Brandon A.D., Huang S. and Leya I. (2013)
Coupled W-Os–Pt isotope systematics in IVB iron meteorites: In situ neutron dosimetry for W isotope chronology. Earth and Planetary Science Letters, 361, 152–161.

Wolff Briche C.S.J., Held A., Berglund M., De Bièvre P. and Taylor P.D.P. (2002)
Measurement of the isotopic composition and atomic weight of an isotopic reference material of platinum, IRMM-010. Analytica Chimica Acta, 460, 41–47.